Video Article

Exploring the Effects of Atmospheric Forcings on Evaporation: Experimental Integration of the Atmospheric Boundary Layer and Shallow Subsurface

Kathleen Smits[1], Victoria Eagen[1], Andrew Trautz[1]

[1]Civil and Environmental Engineering, Colorado School of Mines

Correspondence to: Kathleen Smits at ksmits@mymail.mines.edu

URL: http://www.jove.com/video/52704
DOI: doi:10.3791/52704

Keywords: Environmental Sciences, Issue 100, Bare-soil evaporation, Land-atmosphere interactions, Heat and mass flux, Porous media, Wind tunnel, Soil thermal properties, Multiphase flow

Date Published: 6/8/2015

Citation: Smits, K., Eagen, V., Trautz, A. Exploring the Effects of Atmospheric Forcings on Evaporation: Experimental Integration of the Atmospheric Boundary Layer and Shallow Subsurface. *J. Vis. Exp.* (100), e52704, doi:10.3791/52704 (2015).

Abstract

Evaporation is directly influenced by the interactions between the atmosphere, land surface and soil subsurface. This work aims to experimentally study evaporation under various surface boundary conditions to improve our current understanding and characterization of this multiphase phenomenon as well as to validate numerical heat and mass transfer theories that couple Navier-Stokes flow in the atmosphere and Darcian flow in the porous media. Experimental data were collected using a unique soil tank apparatus interfaced with a small climate controlled wind tunnel. The experimental apparatus was instrumented with a suite of state of the art sensor technologies for the continuous and autonomous collection of soil moisture, soil thermal properties, soil and air temperature, relative humidity, and wind speed. This experimental apparatus can be used to generate data under well controlled boundary conditions, allowing for better control and gathering of accurate data at scales of interest not feasible in the field. Induced airflow at several distinct wind speeds over the soil surface resulted in unique behavior of heat and mass transfer during the different evaporative stages.

Video Link

The video component of this article can be found at http://www.jove.com/video/52704/

Introduction

Understanding the interaction between the land and atmosphere is paramount to our understanding of many current world problems such as leaking of geologically-sequestered carbon dioxide in soil, climate change, water and food supply, the accurate detection of landmines, and the remediation of ground water and soil. In addition, the primary exchanges of heat and water that drive global and regional meteorological conditions occur at the Earth's surface. Many weather and climate phenomena (*e.g.*, hurricanes, El Niño, droughts, *etc.*) are principally driven by processes associated with atmospheric-land surface interactions[1]. As more than half of the land surface on the Earth is arid or semiarid[2-4], accurately describing the water cycle in these regions on the basis of heat and water exchanges between the atmospheric air and the soil surface is critical to improving our understanding of the aforementioned issues, particularly in regions vulnerable to extended drought and desertification. However, despite decades of research, there still remain many knowledge gaps in the current understanding of how the shallow subsurface and atmosphere interact[5].

Transport processes involving liquid water, water vapor, and heat in soil are dynamic and strongly coupled with respect to interactions with the soil and enforced boundary conditions (*i.e.*, temperature, relative humidity, thermal radiation). Numerical heat and mass transfer models commonly oversimplify or overlook a number of these complexities due in part to a lack of testing and refinement of existing theories resulting from a paucity of high temporal and spatial resolution data. Datasets developed for model validation are oftentimes lacking critical atmospheric or subsurface information to properly test the theories, resulting in numerical models that do not properly account for important processes or depend on the use of poorly understood parameters that are adjusted or fitted in the model. This approach is widely used due to its simplicity and ease of use and has in some applications shown much merit. However, this approach can be improved upon by better understanding the physics behind these "lumped parameterizations" by performing well controlled experiments under transient conditions that are capable of testing heat and water transfer theory[6].

Careful experimentation in the laboratory allows precision datasets to be generated that can subsequently be used to validate numerical models. Data available from field sites are often incomplete and costly to obtain, and the degree of control needed to obtain a fundamental understanding of processes and to generate data for model validation could be considered inadequate in some cases. Laboratory experimentation of natural phenomena such as soil evaporation allows atmospheric conditions (*i.e.*, temperature, relative humidity, wind speed) and soil conditions (*i.e.*, soil type, porosity, packing configuration) to be carefully controlled. Many laboratory techniques used to study soil evaporation and soil thermal and hydraulic properties use destructive sampling[7-10]. Destructive sampling methods require that a soil sample be unpacked to obtain point data, preventing the measurement of transient behavior and disrupting soil physical properties; this approach introduces error and uncertainty to the

data. Nondestructive measurements, like the method presented here, allow for more accurate determination and study of the interdependency of soil properties and processes[11].

The goal of this work is to develop a soil tank apparatus and associated protocol for the generation of high spatial and temporal resolution data pertaining to the effects of changes in atmospheric and subsurface conditions on bare-soil evaporation. For this work, a small wind tunnel capable of maintaining a constant wind speed and temperature is interfaced with a soil tank apparatus. The wind tunnel and soil tank are instrumented with a suite of state of the art sensor technologies for autonomous and continuous data collection. Wind speed is measured using a stainless steel pitot-static tube attached to a pressure transducer. Temperature and relative humidity are monitored in the atmosphere using two types of sensors. Relative humidity and temperature are also monitored at the soil surface. Sensors in the subsurface measure soil moisture and temperature. Weight measurements of the tank apparatus are used to determine evaporation through a water mass balance. To demonstrate the applicability of this experimental apparatus and protocol, we present an example of bare-soil evaporation under varying wind speed conditions. The soil tank, packed homogeneously with a well characterized sand, was initially fully saturated and allowed to evaporate freely under carefully controlled atmospheric conditions (*i.e.* temperature, wind speed).

Protocol

Note: Laboratory testing is performed using a two-dimensional bench scale tank interfaced with a climate controlled wind tunnel apparatus. Both the bench scale tank and wind tunnel are instrumented with various sensor technologies. The following protocol will first discuss the construction and preparation of the soil tank, followed by a discussion of the wind tunnel and the instrumentation of both. The tank dimensions, wind tunnel dimensions, number of sensors, and sensor technology type presented can be modified to suit the needs of a specific experimental set-up. The protocol presented below was used to experimentally study the effects of wind speed on bare-soil evaporation.

1. Construction and Preparation of Porous Media Soil Tank

1. Cut a large piece of 1.2 cm thick acrylic glass into five individual panes. Assemble these panes into an open-topped soil tank with internal length, width and height of 25, 9.1 and 55 cm, respectively. Acrylic glass allows processes in the subsurface to be visually observed.
2. Draw a 5 x 5 grid that is 25 cm by 25 cm on each of the two large glass panes (length 25 cm and height 55 cm) as shown in **Figure 1**. Ensure that each square within the grid has an area of 25 cm^2 (**Figure 1**). The grid will be used to properly space the sensors within the soil tank.

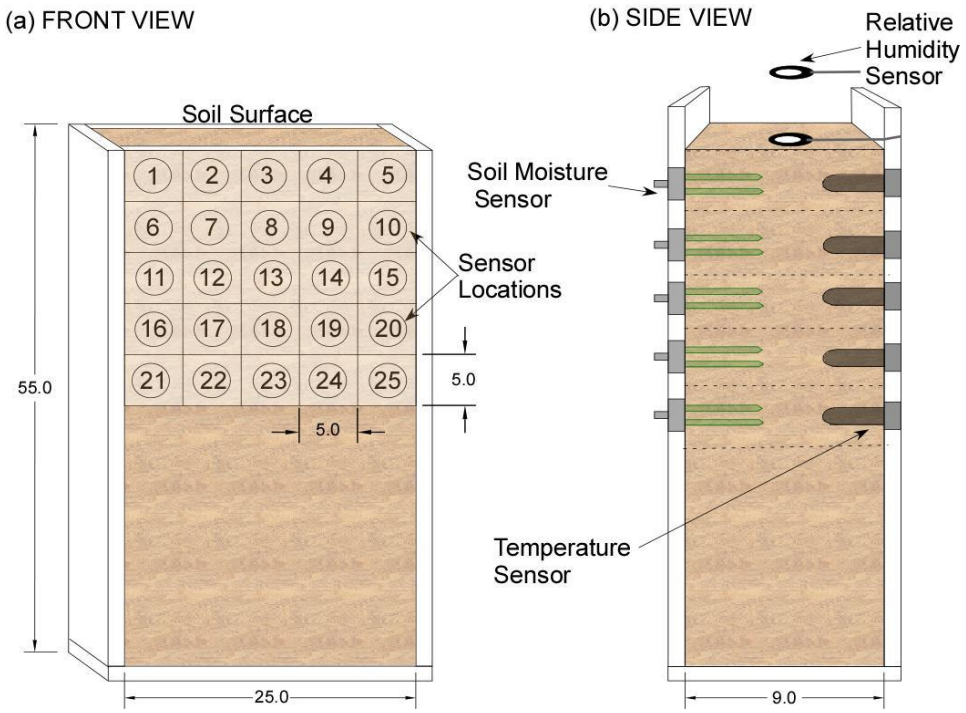

Figure 1: Schematic front and side views of the soil tank used for the experimental set-up (dimensions are in centimeters). (**a**) The front view of the soil tank displaying the grid system consisting of twenty-five 5 cm x 5 cm squares. (**b**) The side view of the soil tank, showing the installed temperature, relative humidity and soil moisture sensor network as a function of depth. Note that the schematics are not drawn to scale.

3. On one of the large glass planes, drill a total of twenty-five 1.9 cm (¾ inch) diameter holes for the soil moisture sensors.
    1. Drill each hole in the center of every square in the grid established in Step 1.2 so that the centers of the holes of two abutting squares are 5 cm apart; the first set of holes is 2.5 cm below the top of the tank. Use appropriately sized taps to cut threads into each of the newly created holes. The 5 cm spacing between sensors ensures that each sensor is outside of the sampling volume of the next closest sensor.

4. Similarly, drill and tap a total of twenty-five 0.635 cm (¼ inch) diameter holes in the center of each grid box created during Step 1.2. Make sure that the center of each hole is spaced 5 cm apart with the first row of holes located 2.5 cm below the top of the soil tank. The 5 cm spacing between sensors ensures that each sensor is outside of the sampling volume of the next closest sensor.
5. On the acrylic pane used as the bottom of the tank, drill and tap a single ½ inch diameter hole in the middle of the pane. Glue a mesh screen (finer than the test soils to be used) over the hole on the internal side of the glass. On the external side of the bottom plane, install a 90° elbow that is attached to flexible tubing with an adjustable valve. This valve and tubing is used to drain water from the tank at the termination of an experiment or as a way to install constant head devices for maintaining constant water table depths.
6. Use marine grade glue or similar water resistant polymer adhesive to attach and seal the tank together as shown in **Figure 1**. Allow the adhesive to cure for one day.
7. To raise the tank off of the ground and make room for the 90° elbow (**Figure 1**), attach two additional pieces of 1.2 cm thick acrylic glass with length 12 cm and height 5 cm to the bottom of the tank.

2. Construction and Preparation of Climate Controlled Wind Tunnel

1. Construct the 215 cm long upstream portion of the wind tunnel out of rectangular galvanized steel ducting material that has a width of 8.5 cm and a height of 26 cm. Surround the outside of the duct with polystyrene insulation.
2. Drill a small hole in the side of the duct work near the downstream exit of the upstream portion of the wind tunnel for the insertion of a relative humidity-temperature sensor (**Figure 2**).

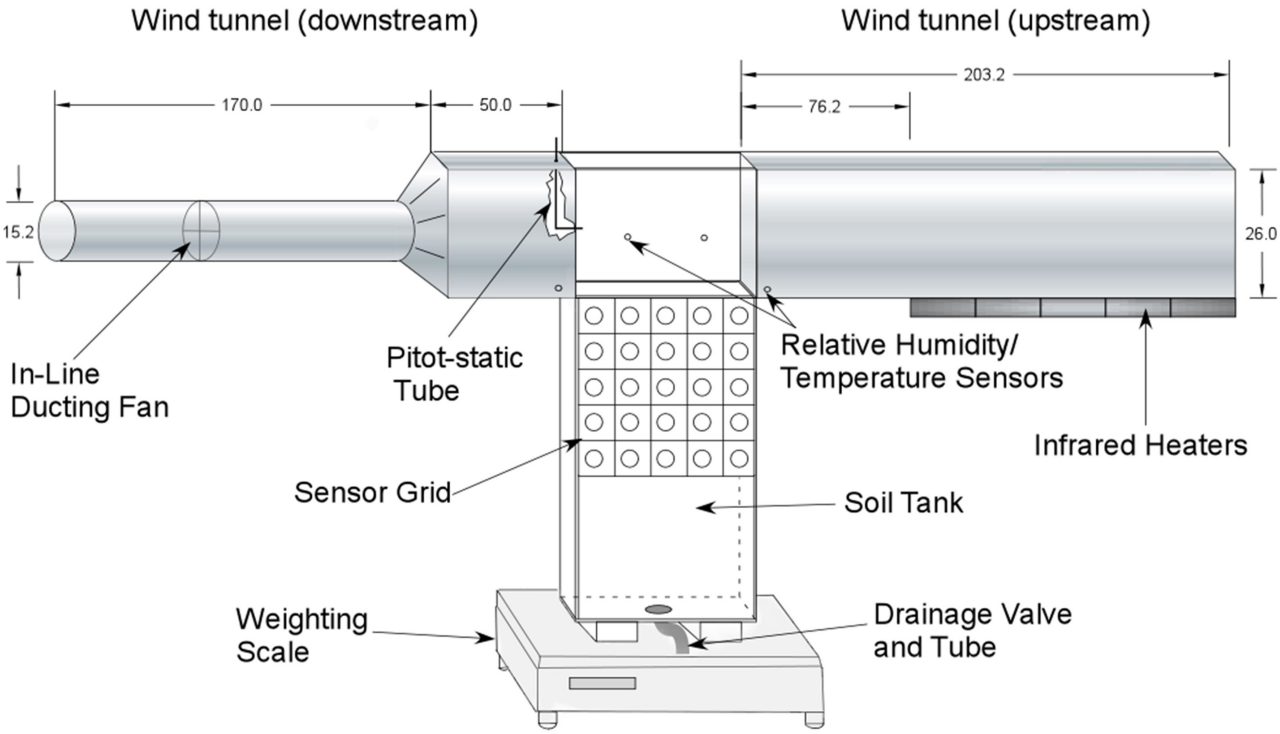

Figure 2: Complete experimental set-up, including tank, ductwork, sensors grid (dimensions are in centimeters). Complete experimental set up of the combined wind tunnel and soil-tank apparatus. The wind tunnel is elevated and sits flush with the surface of the soil tank. The soil tank is instrumented with a network of sensors used to measure a variety of subsurface and atmospheric variables. The grid circles represent the locations for inserting these sensors. A heating control system and an in-line duct fan are used to control temperature and wind speed, respectively. The pitot-static tube is used to measure wind speed. The entire apparatus sits on a weighting scale to obtain a mass balance during experimentation. Note that the schematic is not drawn to scale.

3. Install five ceramic infrared heating elements positioned in parallel within a reflector along the length of the upstream portion of the wind tunnel. Connect the infrared heating elements to a temperature control system regulated by an infrared temperature sensor.
4. Construct the mid-section of the wind tunnel out of two 1.2 cm thick acrylic panels with a length and height of 25 cm and 26 cm respectively. Drill two 0.635 cm (¼ inch) diameter holes in one of the mid-section panels to insert temperature and/or relative humidity-temperature sensors at the locations shown in **Figure 2**.
    1. Secure the acrylic panels to the top of the soil tank side walls (*i.e.*, panels with dimensions 25 cm x 55 cm) using a strong adhesive tape, ensuring that the wind tunnel and soil tank panels sit flush with one another.
5. Construct the first 50 cm of the downstream portion of the wind tunnel out of the same size rectangular ducting material described in Step 2.1. On the terminating side, reduce the rectangular ducting material to a 15.3 cm diameter round duct with length of 170 cm. Install a galvanized steel damper, used to adjust wind speeds, at the far downstream end of the round duct for aid in wind speed control.
6. As in Step 2.2, drill one 0.635 cm diameter hole in the side of the downstream rectangular duct near the entrance for the insertion of a relative humidity-temperature sensor. Drill a second 0.635 cm diameter hole from the top of the rectangular duct along the centerline of the wind tunnel.

7. Install an in-line duct fan in the middle of the round duct (*i.e.*, 85 cm downstream from reduction described in Step 2.4) oriented to expel air from the downstream portion of the wind tunnel. Interface the fan with a variable speed controller for more precise control of rotational frequency and as a result wind speed.
8. Use weldment material and adjustable shelving units to elevate and secure the wind tunnel apparatus. Ensure that the bottom of the upstream and downstream ductwork are flush with the top of the soil tank (**Figure 2**).

3. Installation of Sensors

1. Prior to installation within the soil tank, secure each soil moisture and temperature sensor within a threaded NPT housing (1.9 cm and 0.635 cm housings, respectively) and seal with flashing sealant to prevent moisture intrusion. Do not use silicone-based sealant products as they can interfere with the electronics within some sensors. Cure the sensors for approximately one week.
2. Prior to installation in the soil tank, calibrate the soil moisture sensors in accordance with the two point α-mixing method developed by Sakaki *et al.*[12].
3. Wrap the threads of each NPT housing with plumbers tape prior to installation in the tank to help provide a better seal between the NPT threading and acrylic glass.
4. Install a total of 25 soil moisture and temperature sensors each horizontally through the walls of the tank at the locations discussed in Step 1.2. Twist the sensor cables in sync with the NPT fitting/housing so as not damage the internal wiring within the cables. Do not over-torque the NPTs so as to prevent the glass from cracking. Connect the soil moisture sensors and temperature sensors to their designated data loggers.
5. Install 3 relative humidity-temperature sensors on the soil surface at distances of 2.5, 12.5 and 21.5 cm from the leading edge of the tank. Place the sensors in good contact with the soil surface so that the relative humidity readings reflect the conditions at the soil surface rather than the surrounding air. Connect the sensors to data loggers.
6. To obtain the requisite air temperature and relative humidity measurements in the atmosphere, install relative humidity-temperature sensors in the free flow section of the wind tunnel, using the holes drilled through the upstream and downstream sections of the wind tunnel as well as the panels.
7. Install a pitot-static tube directly downstream of the soil tank through the 0.635 cm hole drilled in the top of the downstream wind tunnel section. Hold the pitot-static tube at a height of 13 cm from the floor of the section. Connect the pitot-static tube to a differential pressure transducer.
8. Calibrate the differential pressure transducer. The pitot-static tube measures dynamic pressure which is defined as the difference of the stagnation and static pressures. The pressure differential is interpreted by the pressure transducer as a voltage differential.
    1. Measure the voltage under no flow conditions (voltage should be approximately equal to 0) and for flow of a known dynamic pressure; this allows a linear relationship to be established between dynamic pressure and voltage. Determine wind speed by applying Bernoulli's equation:
    $$V = \sqrt{\frac{2P_{dynamic}}{\rho}} \quad (1)$$
    where V (m/sec) is wind speed, $P_{dynamic}$ (Pa) is dynamic pressure, and ρ (kg/m^3) is the density of air.
    2. Compare the velocity calculated using Equation (1) with another measurement device. Here, compare the pitot-static tube differential pressure transducer with Laser Doppler Velocimetry (LDV) measurements which has an accuracy of ± 0.01 m/sec.
    Note: A summary of sensors employed and their associated sampling frequencies can be found in **Table 1**. For sensor specifications and other information, refer to the enclosed materials/equipment list.

Sensor	Sensor Measurements	Number of Sensors Employed in Experimental Apparatus	Sensor Sampling Frequency (min)
EC-5	Soil moisture	25	10
ECT	Soil/air temperature	25	10
SH-1	Thermal properties	1	10
EHT	Relative humidity/temperature	5	10
Infrared camera	Surface temperature/evaporation	1	1
Digital camera	Visualization of drying front	1	60
Pitot static tube	Wind velocity	1	10
Weighting scale	Cumulative evaporation/ evaporation rate	1	10

Table 1: Summary of sensors used in experimental portion of present study.

4. Pack the Soil Tank and Prepare for the Start of the Experiment

1. Prior to packing the tank with soil, test its integrity by performing a leak test. Fill the tank with water and wait for 4-6 hr to ensure that no leaks in the structure or sensors have developed.
    1. If leaks develop, drain the tank, let it dry overnight and fix the leaks using the same marine adhesive used during original construction. If no leaks develop, drain the soil tank and prepare for the steps below.

2. Determine the total volume of the tank with sensors in place. Carefully fill the tank with water using a graduated cylinder, making sure to record the amount of water added. Convert the recorded total volume to cubic centimeters for use in Step 4.5.
3. Obtain dry soil to pack the soil tank. Characterize the hydraulic and thermal properties of the selected soil separately in accordance with the methods discussed in Smits *et al.*[11]
4. Carefully wet-pack the soil tank using soil and deionized water.
    1. To wet-pack the soil tank, first pour approximately 5 cm of water into the tank. Slowly add dry soil to the water in the tank, using a scoop, in 2.5 cm depth increments. Record the weight of the sand added during each lift so the porosity of the soil packing can be calculated.
    2. Upon completion of each layer, repeatedly tap the tank walls using a rubber mallet, 100-200 times, to obtain a uniform bulk density throughout. While tapping, avoid contact with the sensors and sensor wires. The use of vibratory devices should be avoided so as not to damage the network of sensitive sensors.
5. Upon completion of packing the tank, sum together the weights of each soil layer (see Step 4.4) to get the total mass of soil. Divide the total mass by the bulk density of soil (*e.g.* the bulk density of quartz sand is 2.65 g/cm^3) to determine the volume of the sand (V_s, cm^3). Calculate the porosity (η, m^3/m^3) of the soil in the tank according to:

$$\eta = \frac{V_T - V_S}{V_T} \quad (2)$$

where (V_T, m^3) is the total volume of the empty tank determined in Step 4.2.
6. Once the tank is fully packed, place a plastic cover such as saran wrap over the tank until the experiment is ready to start to prevent the onset of evaporation.
7. Place the tank on a weighting scale to monitor cumulative water loss which can in turn be used to calculate evaporation rate.
8. Calculate the hourly evaporation rate by dividing the hourly weight loss by the product of the density of water and the cross sectional area of the evaporating surface.

5. Start the Experiment and Begin Data Collection

1. Once the set-up is complete, determine the desired atmospheric conditions (*i.e.* temperature, wind speed). Ensure that the data loggers and other data acquisition systems are turned on and set to the correct sampling intervals (*e.g.*, every 10 min).
2. Start the fan and temperature control system. Allow the climate conditions to equilibrate before removing the plastic cover on the surface of the soil tank. Run the experiment for the desired length of time (*e.g.*, 15 days).

Representative Results

The objective of the experiment presented here was to study the effect of wind speed on evaporation from bare soil. Key properties of the test soil used in the present study are summarized in **Table 2**. A series of experiments were performed in which different boundary conditions at the soil surface (*i.e.*, wind speed and temperature) were applied (**Table 3**). Although four experiments at different wind speeds and temperatures were performed, the majority of experimental results presented here are for a wind speed of 1.22 m/sec. Cumulative evaporation data is shown for all four experiments.

Packing Conditions	Dry Bulk Density (g cm^{-3})	Air Entry Pressure (cm H_2O)	Residual Water Content (m^3 m^{-3})	Van Genuchten Model Parameters *	
				α (cm^{-1})	n (–)
Tight	1.79	16.1/22.5	0.028	0.04	20.53

Table 2: Key properties of experimental test soil used.

Experiment Run #	Average Maximum Wind Velocity	Initial Temperature on Soil surface	Final Temperature on Soil Surface
	(m/sec)	(°C)	(°C)
1	0.55	27	31
2	1.22	26	33
3	3	29	37
4	3.65	33	44.5

Table 3: Experimental wind velocities applied.

Time-dependent relative humidity and temperature measured at the soil surface are presented in **Figure 3**. The relative humidity remains relatively constant at around 0.80 for approximately two days before steeply decreasing over the next four days, beyond which a stable relative humidity value of 0.35 is obtained. The temperature of the soil surface shows an increasing trend over a four-day period before stabilizing. These trends were observed in all four experiments and can be explained in terms of the soil drying. Relative humidity decreases in conjunction with a decrease in evaporation rate because there is less water vapor present over time. The temperature increases as the available water decreases (*i.e.*, evaporation rate decreases) because the process of evaporation no longer cools the soil surface. During the first three days, the relative humidity of downstream air was higher than upstream air due to the presence of more water vapor resulting from upstream evaporation.

This trend was reversed later, most likely due to the upstream sensor losing contact with the soil surface; the sensor cables are flexible and occasionally pull the sensor from the soil surface, changing the humidity reading. The relative humidity measured downstream is greater than that measured upstream because the process of evaporation along the first 21.5 cm of the tank increased the amount of moisture present in air.

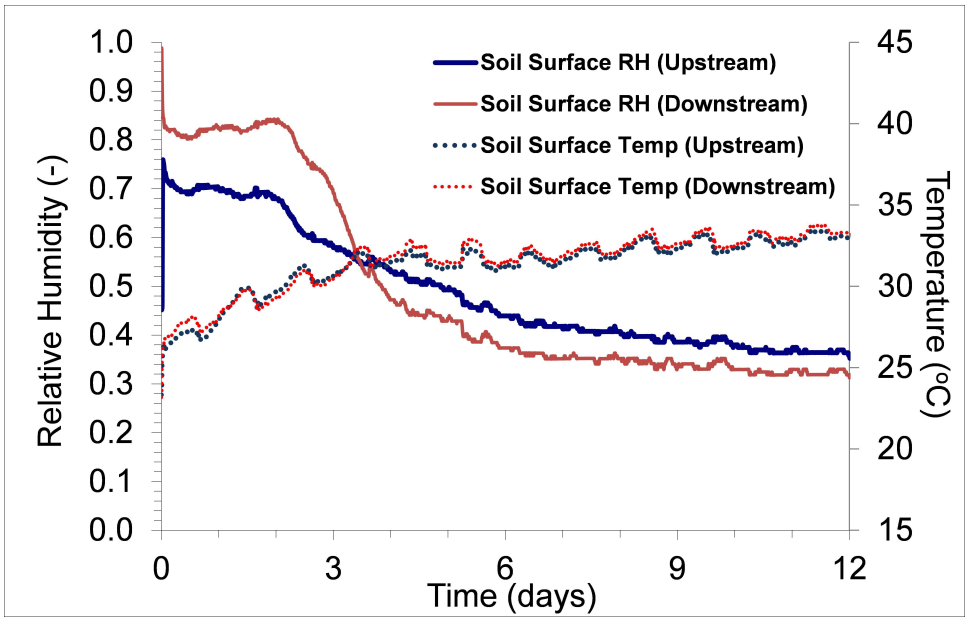

Figure 3: Relative humidity and temperature measured on the soil surface (This figure has been modified from Davarzani *et al.*[5]).

The free flow air temperature in this experiment was set to a constant value of 40 °C using the previously described temperature control system. The time-dependent temperature and relative humidity of the air in the free flow, at a height of 8.5 cm above the soil surface, are shown in **Figure 4**. The observed diurnal fluctuations in temperature are due to the variability of heater outputs in response to the temperature measured by the infrared temperature sensor that regulates the temperature control system (see Step 2.3). Diurnal fluctuations can be avoided, if desired, by setting the infrared temperature sensor to a set temperature value. The difference in atmospheric temperature along the length of the tank is the result of evaporative cooling (**Figure 4**).

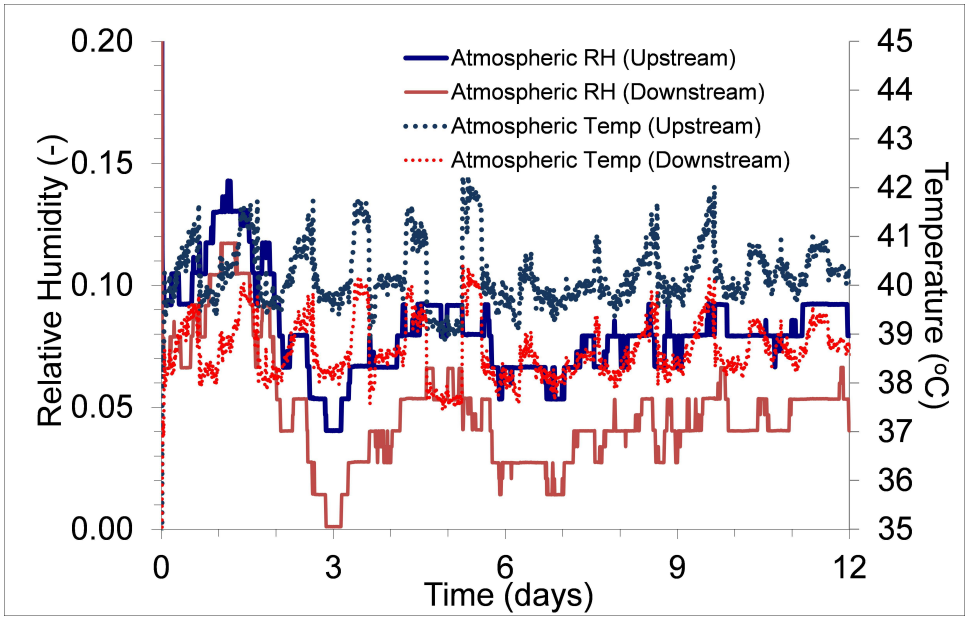

Figure 4: Relative humidity and temperature measured 7.5 cm above the soil surface upstream and downstream of the tank (This figure has been modified from Davarzani *et al.*[5]).

In **Figure 5a**, the time dependent soil temperature is shown for the depths of 2.5 cm, 7.5 cm and 12.5 cm below the soil surface as well as the ambient temperature; see **Figure 1** for sensor identification. As seen in **Figure 5a**, surface temperature and wind velocity are less influential on local temperatures at greater depths — showing no effect at depths below 12.5 cm. **Figure 5b** shows temperature as a function of time for three sensors located at a depth of 2.5 cm. There is a slight difference in temperature for sensors at this depth with the upstream sensor 5 showing

a higher temperature than the downstream Sensor 1. This is because the free flow temperature is always higher upstream than downstream (**Figure 4**). The differences in temperature also results in an asymmetrical saturation profile in the soil tank as will be subsequently shown.

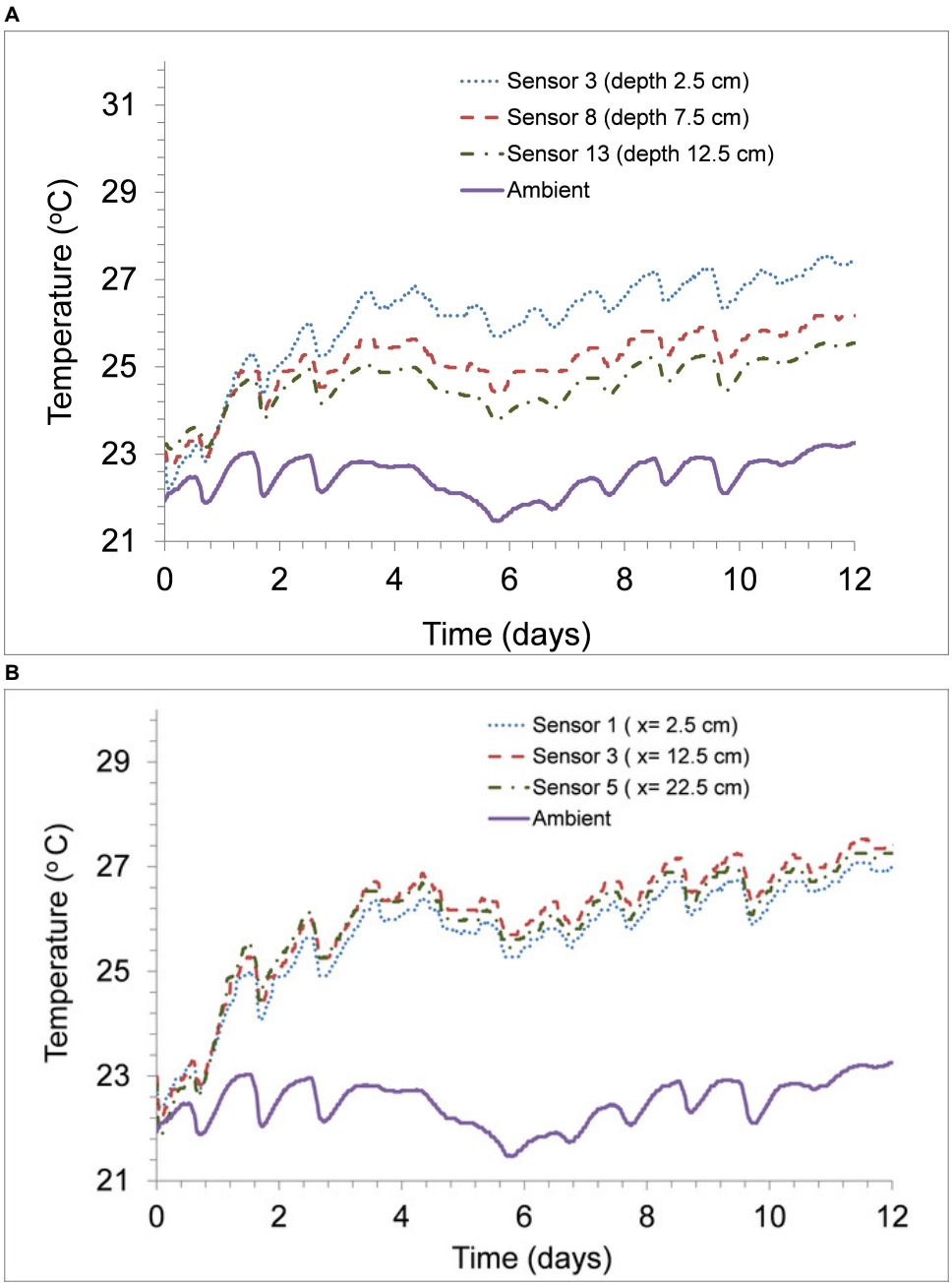

Figure 5: Evolution of measured soil temperature as a function of time (**a**) vertically at the middle of the tank and (**b**) horizontally at a depth of 2.5 cm (This figure has been modified from Davarzani *et al.*[5]).

Figure 6a shows the time-dependent saturation versus time at soil depths of 2.5, 7.5, 12.5, and 17.5 cm. For depths greater than 12.5 cm, the saturation remained at 100% for the duration of the experiment; closer to the soil surface however, saturation decreased over time. The saturation shown in **Figure 6a** can be related to the different stages of evaporation (*i.e.* Stage I and Stage II), defined by differences in evaporation rates, location of the drying front, and dominant transport mechanisms[14]. During Stage I evaporation, the drying front rapidly retreats away from the soil surface as gravitational and viscous forces begin to dominate capillary forces. This is observed in the first day by the measured decrease in soil saturation by the first row of soil moisture sensors corresponding to a depth of 2.5 cm. After Day 1, the rate at which the drying front continues to retreat slows as shown in the gradual shape of the saturation curves for sensors 6-10 located at a depth of 7.5 cm (**Figure 6a**). This marks the transition of evaporation to vapor diffusion limited Stage II evaporation. The initial part of the Stage II is often called the falling rate period[15-17]. Eventually, the saturation curves level out and change very little as the drying front reaches a depth of 12.5 cm (*e.g.*, Sensor 13) by Day 3.

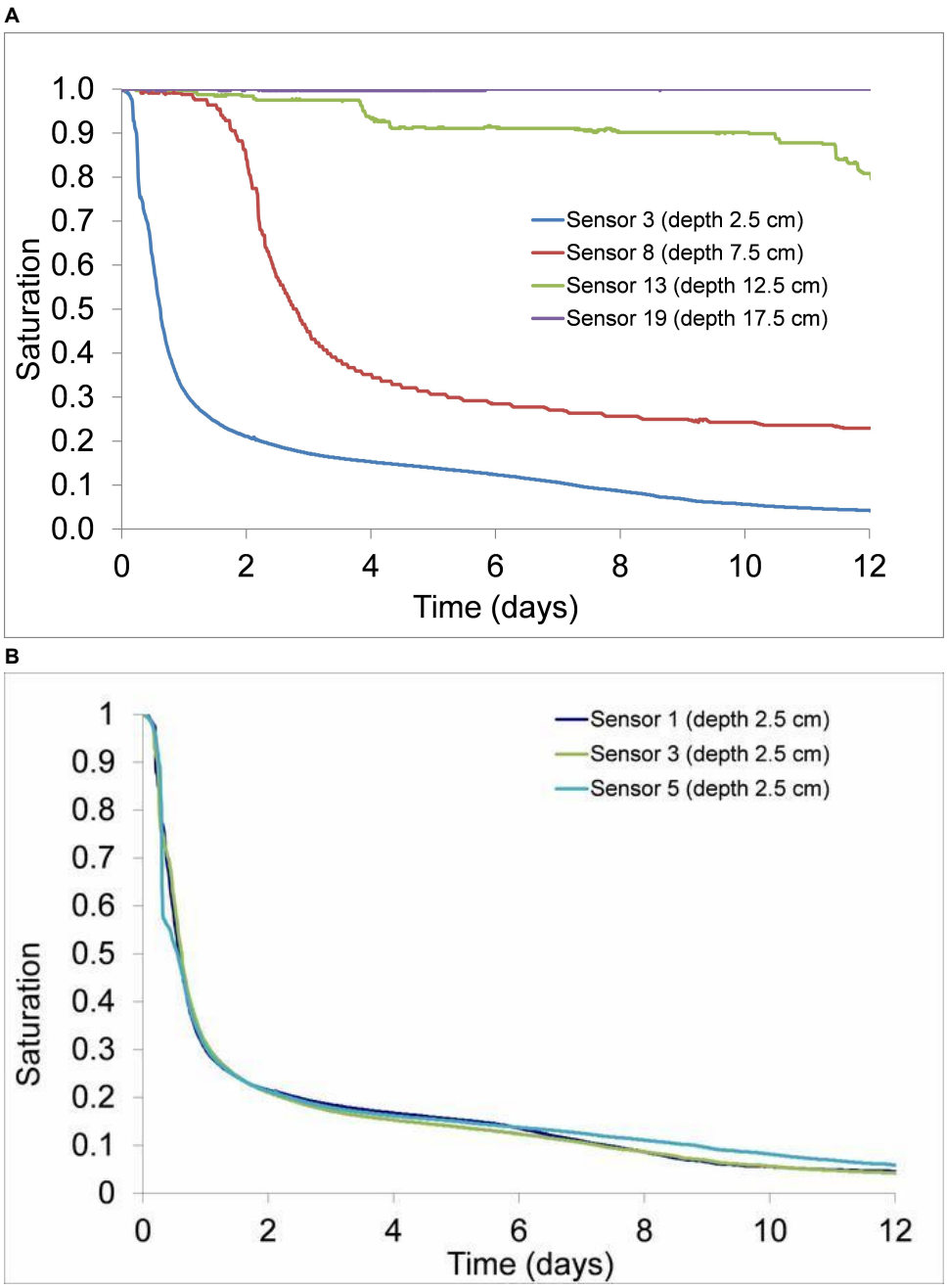

Figure 6: Time evolution of measured subsurface soil saturation (**a**) vertically at the middle of the tank and (**b**) horizontally at a depth of 2.5 cm (This figure has been modified from Davarzani *et al.*[5]).

Figure 6b shows saturation versus time for three sensors located at constant depth of 2.5 cm. The saturation curves are nearly identical and consistent across the entire length of the tank at this depth. The slight asymmetric distribution is due to the air temperature difference between the upstream and downstream sections of the wind tunnel. Since upstream temperatures were consistently a few degrees warmer, atmospheric demand, which drives evaporation, would be higher and therefore there would be a slightly faster rate of drying.

Figure 7 shows wind speed, mean value of 1.22 m/sec, as a function of time. The observed sinusoidal diurnal trend in the wind speed is the result of changes in atmospheric conditions such as barometric pressure and air density. The average wind speed was used in modeling efforts because the effects of diurnal fluctuations of atmospheric variables were not the focus of the present study. This does not mean however, that time-dependent data could not be used. As part of the series of evaporation experiments, four different mean wind velocities were applied; see **Table 3** for a summary. The calculated Reynolds numbers for all experiments in this study were within the laminar and transitional flow regimes. However, it is well know that surface turbulence can affect the evaporation rates[16] and should be addressed in future studies.

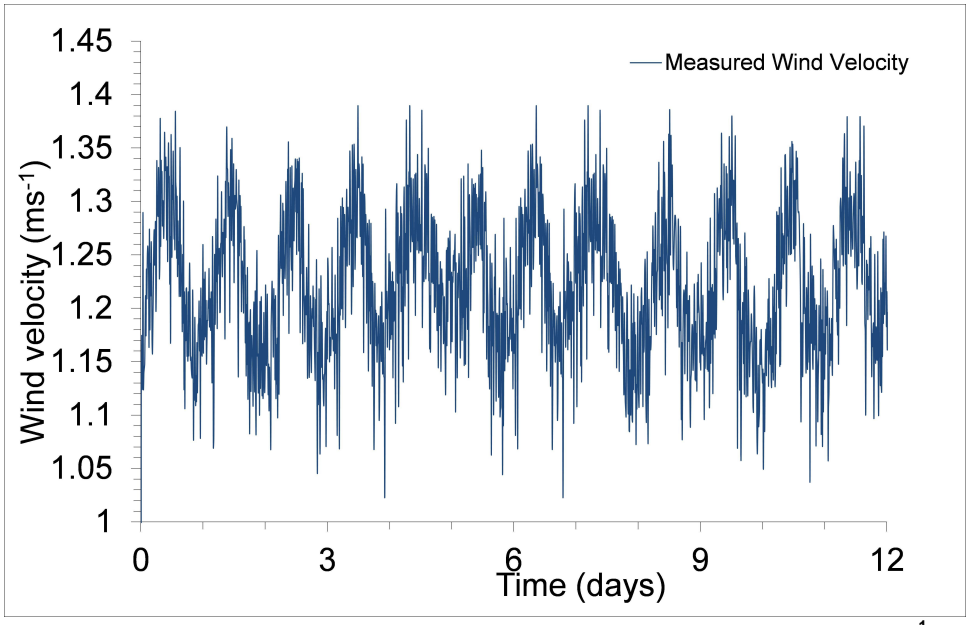

Figure 7: Time-dependent wind speed over the soil surface with mean value of 1.22 m/sec^{-1} (This figure has been modified from Davarzani *et al.*[5])**.**

The effect of the airflow in the free fluid region (*i.e.* atmosphere) on cumulative evaporation is shown in **Figure 8**. Cumulative evaporation is plotted for four different free flow average wind speeds (Vw) of 0.50, 1.20, 3.00 and 3.60 m/sec. Results demonstrate that wind speed has a very prominent effect on cumulative evaporation and the amount of water loss during the different evaporative stages. As shown in **Figure 8**, increasing the wind speed increases the total evaporation. By comparing the slopes of the curves, the greatest influence was on the initial evaporation rate, here referred to as stage 1. Stage 1 evaporation is often defined by high and relatively constant evaporation rates[17] and is predominantly influenced by atmospheric demand rather than soil conditions. As wind speed is further increased from 3 to 3.6 m/sec, evaporation shows much less dependency on incremental changes in wind speed than was observed for changes at low wind speeds. Increasing wind speed leads to an increase in Stage I evaporation rate while simultaneously decreasing the transition time from Stage I to Stage II[5]. The influence of wind speed on evaporation is less significant for Stage II evaporation which is controlled predominantly by the porous medium. During this stage, evaporation is controlled by the rate at which water can be transmitted to the soil surface via diffusion rather than atmospheric demand.

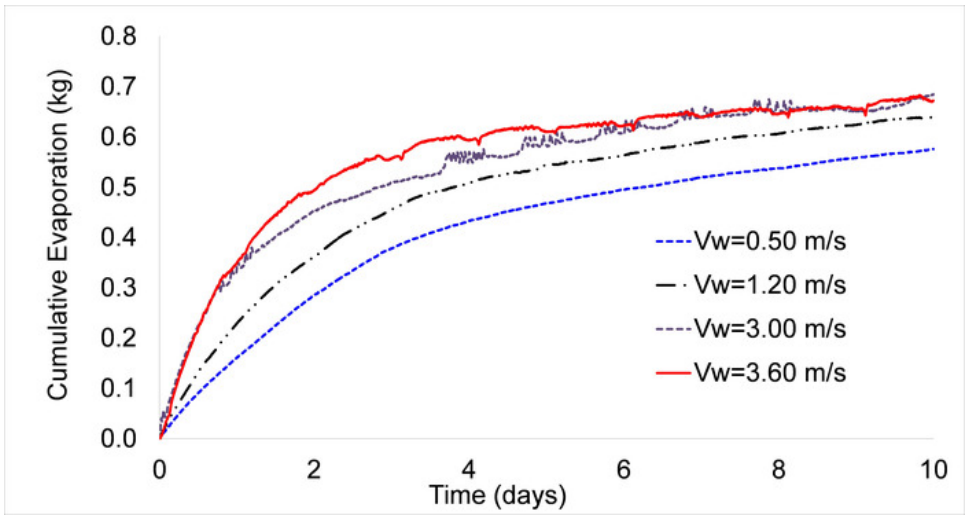

Figure 8: The effect of different mean wind speeds on cumulative evaporation (This figure has been modified from Davarzani *et al.*[5])**.**

Discussion

The purpose of this protocol was to develop an experimental apparatus and associated procedures for the generation of high spatial and temporal resolution data required for studying land-atmospheric interactions with respect to heat and mass transfer processes. The experimental apparatus described consisted of a soil tank and a small wind tunnel, both of which were outfitted with an array of sensors for the measurement of pertinent soil and atmospheric variables (*e.g.*, wind speed, relative humidity, soil and air temperature and soil moisture). The following are some of the most critical components of the protocol presented in this study.

The tank dimensions and sensor placement were specifically chosen to maximize the number of sensors employed while accounting for the sensor's respective sample volumes. The first row of sensors is 2.5 cm below the soil surface due to each sensor's sample volume (defined as the volume of soil around the sensor, within which a change in environmental conditions affects the sensor readings). The sensors, placed in NPT fittings, are installed horizontally through the walls of the soil tank so that the sensor wires are not within the soil itself; all the sensor wires are outside of the tank, preventing water channeling. The installation of a large network of temperature and soil moisture sensors allows horizontal and vertical distributions of these variables to be determined at a fine spatial resolution.

Placing the soil tank on a weighting scale allows cumulative water loss and the associated evaporation rate to be determined using the water mass balance approach described above. These values can then be compared to evaporation rates obtained using other methods such as the combined heat-pulse and sensible heat balance method employed in Trautz *et al.*[18]

The wind tunnel portion of the apparatus is composed of three parts - an upstream, downstream and middle section. The upstream section is used to heat the air before it is drawn over the soil tank in the middle section with the help of a temperature control system. The middle section of the wind tunnel is outfitted with sensor technologies for the measurement of temperature and relative humidity. The downstream portion of the wind tunnel contains an in-line duct fan and damper for controlling wind velocity which is monitored using a pitot-static tube.

The applicability of the soil tank-wind tunnel apparatus described above was demonstrated in an experimental case study of the effects of wind speed on evaporation rate. Results show that increasing wind speed leads to an increased evaporation rate and shortened Stage I evaporation duration. Increasing wind speed beyond 3 m/sec however, shows little additional impact on Stage I evaporation. Stage II evaporation, governed primarily by properties of the porous medium, appears to be independent of or only slightly influenced by wind speed.

This experimental protocol is applicable to a variety of environmental conditions to include changes in soil conditions (*i.e.* different soils, packing configurations, vegetation, and urban environments), climate boundary conditions (temperature, wind speed, precipitation) or subsurface conditions (*e.g.* varying water table levels). The dimensions and sensor layout of the described apparatus can be modified to address the needs of different experiments. The packing procedure described above can similarly be modified to account for different packing configurations such as varying porosity conditions and soil heterogeneity.

Disclosures

The authors declare that they have no competing financial interests.

Acknowledgements

This research was funded by the U. S. Army Research Office Award W911NF-04-1-0169, the Engineering Research and Development Center (ERDC) and National Science Foundation grant EAR-1029069. In addition, this research was supported by a Summer Programs in Undergraduate Research grant from Colorado School of Mines. The authors wish to thank Ryan Tolene and Paul Schulte for their contributions.

References

1. Surface and Planetary Boundary Layer. *Web.* Available from: http://www.esrl.noaa.gov/research/themes/pbl/ (2014).
2. Verstraete, M. M., Schwartz, S. A. Desertification and global change. *Vegetatio.* **91**, 3-13 (1991).
3. Warren, A. Desertification. *The Physical Geography of Africa.* Adams, W. M., Goudie, A. S., Orme, A. R. 342-355 University Press Oxford (1996).
4. Katata, G., Nagai, H., Ueda, H., Agam, N., Berliner, P. R. Development of a land surface model including evaporation and adsorption processes in the soil for the land-air exchange in arid regions. *J. Hydrometeorol.* **8**, 1307-1324 (2007).
5. Davarzani, H., Smits, K. M., Tolene, R., Illangasekare, T. H. Study of the effect of wind speed on evaporation from soil through integrated modeling of atmospheric boundary layer and shallow subsurface. *Water Resour. Res.* **50**, (2014).
6. Heitman, J. L., Horton, R., Ren, T., Nassar, I. N., Davis, D. D. A test of coupled soil heat and water transfer prediction under transient boundary temperatures. *Soil Sci. Soc. Am. J.* **72**, (5), 1197-1207 (2008).
7. Gurr, C. G., Marshall, T. J., Hutton, J. T. Movement of water in soil due to a temperature gradient. *Soil Sci.* **74**, 335-345 (1952).
8. Nassar, I. N., Horton, R. Water transport in unsaturated non-isothermal salty soil: experimental results. *Soil Sci. Soc. Am. J.* **53**, 1323-1363 (1989).
9. Prunty, L., Horton, R. Steady-state Temperature Distribution in Nonisothermal unsaturated closed soil cells. *Soil Sci. Soc. Am. J.* **58**, 1358-1363 (1994).
10. Bachmann, J., Horton, R., Ren, T., van der Ploeg, R. R. Comparison of the thermal properties of four wettable and four water-repellent soils. *Soil Sci. Soc. Am. J.* **65**, (6), 1675-1679 (2001).
11. Smits, K. M., Sakaki, T., Limsuwat, A., Illangasekare, T. H. Thermal conductivity of sands under varying moisture and porosity in drainage-wetting cycles. *Vadose Zone J.* **9**, 1-9 (2010).
12. Sakaki, T., Limsuwat, A., Smits, K. M., Illangasekare, T. H. Empirical two-point α-mixing Model for calibrating the ECH2O EC-5 soil sensor in sands. *Water Resources Research.* **44**, W00D08 (2008).
13. Shokri, N., Lehmann, P., Or, D. Evaporation from layered porous media. *J. Geophys. Res.* **115**, B06204 (2010).
14. Van Brakel, J. Mass transfer in convective drying. *Advances in Drying.* Mujumdar, A. S. **1**, 217-267 (1980).
15. Yiotis, A. G., Subos, A. G. B. oudouvisA. K., Tsimpanogiannis, I. N., Yortsos, Y. C. The effect of liquid films on the drying of porous media. *AIChE J.* **50**, 2721-2737 (2004).
16. Ishihara, Y., Shimojima, E., Harada, H. Water vapor transfer beneath bare soil where evaporation is influenced by a turbulent surface wind. *J. Hydrol.* **131**, (1-4), 63-104 (1992).
17. Lehmann, P., Assouline, S., Or, D. Characteristic lengths affecting evaporative drying of porous media. *Phys. Rev. E.* **77**, (5 Pt 2), 056309 (2008).

18. Trautz, A. C., Smits, K. M., Schulte, P., Illangasekare, T. H. Sensible heat balance and heat-pulse method applicability to in situ soil-water evaporation. *Vadose Zone J.* **13**, (2014).

